

Improved bounds on the dipole moments of the tau-neutrino at high-energy γ^*e^- and $\gamma^*\gamma^*$ collisions: ILC and CLIC

A. Gutiérrez-Rodríguez*,¹ M. Koksall†,² and A. A. Billur‡²

¹*Facultad de Física, Universidad Autónoma de Zacatecas*

Apartado Postal C-580, 98060 Zacatecas, México.

²*Department of Physics, Cumhuriyet University, 58140, Sivas, Turkey.*

(Dated: October 27, 2018)

Abstract

In this work we probing the potential of the processes $e^+e^- \rightarrow e^+\gamma^*e^- \rightarrow e^+\tau\bar{\nu}_\tau\nu_e$ and $e^+e^- \rightarrow e^+\gamma^*\gamma^*e^- \rightarrow e^+\nu_\tau\bar{\nu}_\tau e^-$ at a future high-energy and high-luminosity linear electron positron collider, such as the ILC and CLIC to study the sensibility on the anomalous magnetic and electric dipole moments of the tau-neutrino. For integrated luminosity of 590 fb^{-1} and center-of-mass energy of 3 TeV , we derive 95% *C.L.* limits on the dipole moments: $\mu_{\nu_\tau} \leq 1.33 \times 10^{-6} \mu_B$ and $d_{\nu_\tau} \leq 2.56 \times 10^{-17} \text{ e cm}$ in the γ^*e^- collision mode and of $\mu_{\nu_\tau} \leq 3.4 \times 10^{-7} \mu_B$ and $d_{\nu_\tau} \leq 6.56 \times 10^{-18} \text{ e cm}$ with the $\gamma^*\gamma^*$ collision mode, improving the existing limits.

PACS numbers: 14.60.St, 13.40.Em

Keywords: Non-standard-model neutrinos, Electric and Magnetic Moments.

* alexgu@fisica.uaz.edu.mx

† mkoksall@cumhuriyet.edu.tr

‡ abillur@cumhuriyet.edu.tr

I. INTRODUCTION

In the Standard Model (SM) [1–3] extended to contain right-handed neutrinos, the neutrino magnetic moment induced by radiative corrections is unobservably small, $\mu_\nu = 3eG_F m_{\nu_i}/(8\sqrt{2}\pi^2) \simeq 3.1 \times 10^{-19}(m_{\nu_i}/1 \text{ eV})\mu_B$, where $\mu_B = e/2m_e$ is the Bohr magneton [4]. Current limits on these magnetic moments are several orders of magnitude larger, so that a magnetic moment close to these limits would indicate a window for probing effects induced by new physics beyond the SM [5]. Similarly, a neutrino electric dipole moment will also point to new physics and will be of relevance in astrophysics and cosmology, as well as terrestrial neutrino experiments [6]. The tau-neutrino electromagnetic vertex may be parameterized in the following form:

$$\Gamma^\alpha = eF_1(q^2)\gamma^\alpha + \frac{ie}{2m_{\nu_\tau}}F_2(q^2)\sigma^{\alpha\mu}q_\mu + eF_3(q^2)\gamma_5\sigma^{\alpha\mu}q_\mu, \quad (1)$$

where e is the charge of the electron, m_{ν_τ} is the mass of the tau-neutrino, q^μ is the photon momentum, and $F_{1,2,3}(q^2)$ are the electromagnetic form factors of the neutrino, corresponding to charge radius, magnetic moment (MM) and electric dipole moment (EDM), respectively, at $q^2 = 0$ [7, 8].

The current best limit on μ_{ν_τ} has been obtained in the Borexino experiment which explores solar neutrinos. Searches for magnetic moment of the tau-neutrino have been performed also in accelerator experiments. The experiment E872 (DONUT) is based at $\nu_\tau e^-, \bar{\nu}_\tau e^-$ elastic scattering. In the CERN experiment WA-066, a limit on μ_{ν_τ} is obtained on an assumed flux of tau-neutrinos in the neutrino beam. The L3 collaboration obtain a limit on the magnetic moment of the tau-neutrino from a sample of e^+e^- annihilation events at the Z resonance. Experimental limits on the magnetic moment of the tau-neutrino are shown in Table I.

Others limits on the magnetic moment of the μ_{ν_τ} are reported in the literature [7, 13–31].

In this work we study the sensibility on the anomalous magnetic and electric dipole moments of the tau-neutrino through of the processes $e^+e^- \rightarrow e^+\gamma^*e^- \rightarrow e^+\tau\bar{\nu}_\tau\nu_e$ and $e^+e^- \rightarrow e^+\gamma^*\gamma^*e^- \rightarrow e^+\nu_\tau\bar{\nu}_\tau e^-$ at a future high-energy and high-luminosity linear electron positron collider, with a center-of-mass energy in the range of 500 to 1600 GeV , such as the International Linear Collider (ILC) [32], and of 3 TeV to the Compact Linear Collider (CLIC) [33]. The future e^+e^- linear collider cannot only be designed to operate in e^+e^-

TABLE I: Experimental limits on the magnetic moment of the tau-neutrino.

Experiment	Method	Limit	C. L.	Reference
Borexino	Solar neutrino	$\mu_{\nu_\tau} < 1.9 \times 10^{-10} \mu_B$	90%	[9]
E872 (DONUT)	Accelerator $\nu_\tau e^-, \bar{\nu}_\tau e^-$	$\mu_{\nu_\tau} < 3.9 \times 10^{-7} \mu_B$	90%	[10]
CERN-WA-066	Accelerator	$\mu_{\nu_\tau} < 5.4 \times 10^{-7} \mu_B$	90%	[11]
L3	Accelerator	$\mu_{\nu_\tau} < 3.3 \times 10^{-6} \mu_B$	90%	[12]

collision mode, but can also be operated as a $e\gamma$ and $\gamma\gamma$ collider. This is achieved by using Compton backscattered photons in the scattering of intense laser photons on the initial e^+e^- beams. The other well-known applications of linear colliders are to study new physics beyond the SM through $e\gamma^*$ and $\gamma^*\gamma^*$ collisions. A quasi-real γ^* photon emitted from one of the incoming e^- or e^+ beams can interact with the other lepton shortly after, and the subprocess $\gamma^*e^- \rightarrow \tau\bar{\nu}_\tau\nu_e$ can generate. Hence, first, we calculate the main reaction $e^+e^- \rightarrow e^+\gamma^*e^- \rightarrow e^+\tau\bar{\nu}_\tau\nu_e$ by integrating the cross section for the subprocess $\gamma^*e^- \rightarrow \tau\bar{\nu}_\tau\nu_e$. Also, γ^* photons emitted from both e^- and e^+ beams collide with each other, and the subprocess $\gamma^*\gamma^* \rightarrow \nu_\tau\bar{\nu}_\tau$ can be produced. Second, we find the main reaction $e^+e^- \rightarrow e^+\gamma^*\gamma^*e^- \rightarrow e^+\nu_\tau\bar{\nu}_\tau e^-$ by integrating the cross section for the subprocess $\gamma^*\gamma^* \rightarrow \nu_\tau\bar{\nu}_\tau$. Quasi-real photons in $e\gamma^*$ and $\gamma^*\gamma^*$ collisions can be examined by Equivalent Photon Approximation (EPA) [34–36], that is to say, using the Weizsacker-Williams approximation. In EPA, photons emitted from incoming leptons which have very low virtuality are scattered at very small angles from the beam pipe. Because the emitted quasi-real photons have a low Q^2 virtuality. Therefore they are almost real. These processes have been observed experimentally at the LEP, Tevatron and LHC [37–43]. Especially, the most stringent experimental limit on the anomalous magnetic dipole moment of the tau lepton is obtained through the process $e^+e^- \rightarrow e^+\gamma^*\gamma^*e^- \rightarrow e^+\tau\bar{\tau}e^-$ by using multiperipheral collision at the LEP [44].

In Refs. [45, 46], the electromagnetic properties of the neutrinos were examined via the Weizsacker-Williams approximation at the LHC. Ref. [45] was investigated nonstandard $\nu\bar{\nu}\gamma$ and $\nu\bar{\nu}\gamma\gamma$ couplings via $\nu\bar{\nu}q$ production in the process $pp \rightarrow p\gamma^*p \rightarrow p\nu\bar{\nu}qX$. In addition, the potential of $\gamma^*\gamma^*$ collisions at the LHC was studied via the reaction $pp \rightarrow p\gamma^*\gamma^*p \rightarrow p\nu\bar{\nu}p$ to probe neutrino-photon coupling by Ref. [46].

With these motivations, we probing the potential of the processes $e^+e^- \rightarrow e^+\gamma^*e^- \rightarrow e^+\tau\bar{\nu}_\tau\nu_e$ and $e^+e^- \rightarrow e^+\gamma^*\gamma^*e^- \rightarrow e^+\nu_\tau\bar{\nu}_\tau e^-$ and derive limits on the dipole moments μ_{ν_τ} and d_{ν_τ} at 2σ and 3σ level (90% and 95% C.L.) via Weisacker-Williams approximation, and at a future high-energy and high-luminosity linear electron positron collider, such as the ILC and CLIC to study the sensibility on the anomalous magnetic and electric dipole moments of the tau-neutrino.

For this we calculate the main reaction $e^+e^- \rightarrow e^+\gamma^*e^- \rightarrow e^+\tau\bar{\nu}_\tau\nu_e$ by integrating the cross section for the subprocess $\gamma^*e^- \rightarrow \tau\bar{\nu}_\tau\nu_e$. The acceptance cuts will imposed as $|\eta^\tau| < 2.5$ for pseudorapidity and $p_T^\tau > 20 \text{ GeV}$ for transverse momentum cut of the final state τ lepton, respectively. For the second process we calculate the main reaction $e^+e^- \rightarrow e^+\gamma^*\gamma^*e^- \rightarrow e^+\nu_\tau\bar{\nu}_\tau e^-$. Neutrinos in this process are not detected directly in the central detector. Therefore we do not apply any cuts for the final state particles. The corresponding Feynman diagrams for the main reactions as well as for the sub-processes which give the most important contribution to the total cross-section are shown in Figs. 1-4.

To illustrate our results for both processes we show the dependence of the total cross-section as a function of anomalous couplings F_2 and F_3 for three different values of the center-of-mass energies 0.5, 1.5 and 3 TeV , respectively. The variation of the cross-section as a function of F_2 and F_3 for different values of Q^2 (Weizsacker-Williams photon virtuality) and center-of-mass energy of 0.5, 1.5 and 3 TeV is evaluated. We also include a contours plot for the upper bounds of the anomalous couplings μ_{ν_τ} and d_{ν_τ} with 95% C.L. at the $\sqrt{s} = 0.5, 1.5, 3 \text{ TeV}$ with corresponding maximum luminosities for both processes. The sensitivity limits on the magnetic moment μ_{ν_τ} and the electric dipole moment d_{ν_τ} of the tau-neutrino for different values of photon virtuality, center-of-mass energy and luminosity are also calculated.

This paper is organized as follows. In Section II, we study the dipole moments of the tau-neutrino through the processes $e^+e^- \rightarrow e^+\gamma^*e^- \rightarrow e^+\tau\bar{\nu}_\tau\nu_e$ in the γ^*e^- collision mode and $e^+e^- \rightarrow e^+\gamma^*\gamma^*e^- \rightarrow e^+\nu_\tau\bar{\nu}_\tau e^-$ through the $\gamma^*\gamma^*$ collision mode. Finally, we summarize our conclusions in Section III.

II. CROSS-SECTION OF $e^+e^- \rightarrow e^+\gamma^*e^- \rightarrow e^+\tau\bar{\nu}_\tau\nu_e$ AND $e^+e^- \rightarrow e^+\gamma^*\gamma^*e^- \rightarrow e^+\nu_\tau\bar{\nu}_\tau e^-$

In this section we present numerical results of the cross-section for both processes $e^+e^- \rightarrow e^+\gamma^*e^- \rightarrow e^+\tau\bar{\nu}_\tau\nu_e$ and $e^+e^- \rightarrow e^+\gamma^*\gamma^*e^- \rightarrow e^+\nu_\tau\bar{\nu}_\tau e^-$ as a function of the electromagnetic form factors of the neutrino F_2 and F_3 . In addition to see the sensitivity of the magnetic moment μ_{ν_τ} and the electric dipole moment d_{ν_τ} to new physics, we plot the luminosity \mathcal{L} versus $\mu_{\nu_\tau}(d_{\nu_\tau})$. We carry out the calculations using the framework of the minimally extended standard model at next generation linear γ^*e^- and $\gamma^*\gamma^*$ collisions: ILC and CLIC.

We use the CompHEP [47] packages for calculations of the matrix elements and cross-sections. These packages provide automatic computation of the cross-sections and distributions in the SM as well as their extensions at tree-level. We consider the high energy stage of possible future linear γ^*e^- and $\gamma^*\gamma^*$ collisions with $\sqrt{s} = 0.5, 1.5$ and 3 TeV and design luminosity 230, 320 and 590 fb^{-1} according to the data reported by the ILC and CLIC [32, 33]. In addition, we consider the acceptance cuts of $|\eta^\tau| < 2.5$ for pseudorapidity and $p_T^\tau > 20 \text{ GeV}$ for transverse momentum cut of the final state τ lepton, respectively.

A. Magnetic moment and electric dipole moment via $e^+e^- \rightarrow e^+\gamma^*e^- \rightarrow e^+\tau\bar{\nu}_\tau\nu_e$

To illustrate our results we show the dependence of the cross-section on the anomalous couplings F_2 and F_3 for $e^+e^- \rightarrow e^+\gamma^*e^- \rightarrow e^+\tau\bar{\nu}_\tau\nu_e$ in Fig. 5 for three different center-of-mass energies $\sqrt{s} = 0.5, 1.5, 3 \text{ TeV}$ and $Q^2 = 2, 16, 64 \text{ GeV}^2$, respectively. The cross-section is sensitive to the value of the center-of-mass energies, as well as to Q^2 . The sensitivity to $e^+\tau\bar{\nu}_\tau\nu_e$ increases with the collider energy, as well as with Q^2 reaching a maximum at the end of the range considered: $F_{2,3} = \pm 0.001$. In Fig. 6, we show again the total cross-section, but now for different values of $Q^2 = 2, 16, 64 \text{ GeV}^2$ and center-of-mass energies of $\sqrt{s} = 0.5, 1.5, 3 \text{ TeV}$. We observed that the variation of the cross-section for $e^+\tau\bar{\nu}_\tau\nu_e$ as a function of the anomalous couplings F_2 and F_3 it is clear for all case.

In Figures 7 and 8 we present the dependence of the sensitivity limits of the magnetic moment μ_{ν_τ} and the electric dipole moment d_{ν_τ} with respect to the collider luminosity \mathcal{L} for three different values of the Weizsacker-Williams photon virtuality $Q^2 = 2, 16, 64 \text{ GeV}^2$ and center-of-mass energies of $\sqrt{s} = 0.5, 1.5, 3 \text{ TeV}$.

As an indicator of the order of magnitude, in Tables II-III we present the bounds obtained on the μ_{ν_τ} magnetic moment and d_{ν_τ} electric dipole moment for $Q^2 = 2, 64 \text{ GeV}^2$, $\sqrt{s} = 0.5, 1.5, 3 \text{ TeV}$ and $\mathcal{L} = 230, 320, 590 \text{ fb}^{-1}$ at 2σ and $3\sigma \text{ C.L.}$, respectively. We observed that the results obtained in Tables II and III are competitive with those reported in the literature [10–12]. For the electric dipole moment our limits compare favorably with those reported by K. Akama, *et al.* [23] $|d_{\nu_\tau}| < O(2 \times 10^{-17} \text{ ecm})$ and R. Escribano, *et al.* [7] $|d_{\nu_\tau}| \leq 5.2 \times 10^{-17} \text{ ecm}$, 95% C.L.

In Fig. 9 we used three center-of-mass energies $\sqrt{s} = 0.5, 1.5, 3 \text{ TeV}$ planned for ILC/CLIC accelerators in order to get contours limits in the plane $\mu_{\nu_\tau} - d_{\nu_\tau}$ for $e^+e^- \rightarrow e^+\gamma^*e^- \rightarrow e^+\tau\bar{\nu}_\tau\nu_e$ and the planned luminosities of $\mathcal{L} = 230, 320, 590 \text{ fb}^{-1}$ and Weizsacker-Williams photon virtuality $Q^2 = 2 \text{ GeV}^2$. For the γ^*e^- collision, we perform χ^2 analysis at 95% C.L. since the number of SM events is greater than 10.

TABLE II: Bounds on the μ_{ν_τ} magnetic moment and d_{ν_τ} electric dipole moment for the process $e^+e^- \rightarrow e^+\gamma^*e^- \rightarrow e^+\tau\bar{\nu}_\tau\nu_e$ for $Q^2 = 2 \text{ GeV}^2$, $\sqrt{s} = 0.5, 1.5, 3 \text{ TeV}$ and $\mathcal{L} = 230, 320, 590 \text{ fb}^{-1}$ at 2σ and $3\sigma \text{ C. L.}$

$\sqrt{s} = 0.5, 1.5, 3 \text{ TeV}, \quad \mathcal{L} = 230, 320, 590 \text{ fb}^{-1}$		
C. L.	$ \mu_{\nu_\tau}(\mu_B) $	$ d_{\nu_\tau}(\text{ecm}) $
2σ	$(8.71, 3.14, 1.54) \times 10^{-6}$	$1.68 \times 10^{-16}, (6.07, 2.98) \times 10^{-17}$
3σ	$(9.27, 3.07, 1.46) \times 10^{-6}$	$1.79 \times 10^{-16}, (5.92, 2.82) \times 10^{-17}$

TABLE III: Bounds on the μ_{ν_τ} magnetic moment and d_{ν_τ} electric dipole moment for the process $e^+e^- \rightarrow e^+\gamma^*e^- \rightarrow e^+\tau\bar{\nu}_\tau\nu_e$ for $Q^2 = 64 \text{ GeV}^2$, $\sqrt{s} = 0.5, 1.5, 3 \text{ TeV}$ and $\mathcal{L} = 230, 320, 590 \text{ fb}^{-1}$ at 2σ and $3\sigma \text{ C. L.}$

$\sqrt{s} = 0.5, 1.5, 3 \text{ TeV}, \quad \mathcal{L} = 230, 320, 590 \text{ fb}^{-1}$		
C. L.	$ \mu_{\nu_\tau}(\mu_B) $	$ d_{\nu_\tau}(\text{ecm}) $
2σ	$(7.65, 2.71, 1.35) \times 10^{-6}$	$1.47 \times 10^{-16}, (5.22, 2.61) \times 10^{-17}$
3σ	$(8.18, 2.77, 1.33) \times 10^{-6}$	$1.58 \times 10^{-16}, (5.35, 2.56) \times 10^{-17}$

B. Magnetic moment and electric dipole moment via $e^+e^- \rightarrow e^+\gamma^*\gamma^*e^- \rightarrow e^+\nu_\tau\bar{\nu}_\tau e^-$

In this subsection we study the dipole moments of the tau-neutrino via the processes $e^+e^- \rightarrow e^+\gamma^*\gamma^*e^- \rightarrow e^+\nu_\tau\bar{\nu}_\tau e^-$ for energies expected at the ILC and CLIC [32, 33]. Figure 10 show the total cross-section as a function of the electromagnetic form factors of the neutrino F_2 and F_3 for three different center-of-mass energies $\sqrt{s} = 0.5, 1.5, 3 \text{ TeV}$ and $Q^2 = 2, 16, 64 \text{ GeV}^2$, respectively. We can see from this figure that the total cross-section changes strongly with the variation of the \sqrt{s} and Q^2 values.

As in subsection A, we show the F_2 and F_3 dependence of the total cross-section for $e^+e^- \rightarrow e^+\gamma^*\gamma^*e^- \rightarrow e^+\nu_\tau\bar{\nu}_\tau e^-$ in Fig. 11. From this figure we observed a significantly dependence of the cross-section with respect to F_2 and F_3 , and different values of center-of-mass energy \sqrt{s} and Q^2 . In Figures 12 and 13 we present the dependence of the sensitivity limits of the magnetic moment μ_{ν_τ} and the electric dipole moment d_{ν_τ} with respect to the collider luminosity \mathcal{L} for three different values of $Q^2 = 2, 16, 64 \text{ GeV}^2$ and center-of-mass energies of $\sqrt{s} = 0.5, 1.5, 3 \text{ TeV}$.

In Tables IV and V we present the bounds obtained on the μ_{ν_τ} magnetic moment and d_{ν_τ} electric dipole moment for $\sqrt{s} = 0.5, 1.5, 3 \text{ TeV}$, $Q^2 = 2, 64 \text{ GeV}^2$ and $\mathcal{L} = 230, 320, 590 \text{ fb}^{-1}$ at 2σ and 3σ . We observed that the results obtained in Tables IV-V improve the bounds reported in the literature [10–12].

In the case of the electric dipole moment the 90, 95% C. L. sensitivity limits at 0.5, 1.5 and 3 TeV center of mass energies and integrated luminosities of 230, 320 and 590 fb^{-1} , respectively can provide proof of these bounds of order 10^{-18} , that is to say, are improved by one order of magnitude than those reported in the literature: $|d_{\nu_\tau}| < O(2 \times 10^{-17} \text{ ecm})$ [23] and $|d_{\nu_\tau}| \leq 5.2 \times 10^{-17} \text{ ecm}$, 95% C. L. [7].

Finally, in Fig. 14 we summarize the respective limit contours for the dipole moments in the $\mu_{\nu_\tau} - d_{\nu_\tau}$ plane for $e^+e^- \rightarrow e^+\gamma^*\gamma^*e^- \rightarrow e^+\nu_\tau\bar{\nu}_\tau e^-$. Starting from the top, the curves are for $\sqrt{s} = 0.5 \text{ TeV}$ and $\mathcal{L} = 230 \text{ fb}^{-1}$; $\sqrt{s} = 1.5 \text{ TeV}$ and $\mathcal{L} = 320 \text{ fb}^{-1}$; $\sqrt{s} = 3 \text{ TeV}$ and $\mathcal{L} = 590 \text{ fb}^{-1}$, respectively. We have used $Q^2 = 2 \text{ GeV}^2$. In this case for the $\gamma^*\gamma^*$ collision, we perform Poisson analysis at 95% C.L. since the number of SM events is smaller than 10.

TABLE IV: Bounds on the μ_{ν_τ} magnetic moment and d_{ν_τ} electric dipole moment for the process $e^+e^- \rightarrow e^+\gamma^*\gamma^*e^- \rightarrow e^+\nu_\tau\bar{\nu}_\tau e^-$ for $Q^2 = 2 \text{ GeV}^2$, $\sqrt{s} = 0.5, 1.5, 3 \text{ TeV}$ and $\mathcal{L} = 230, 320, 590 \text{ fb}^{-1}$ at 2σ and 3σ C. L.

$\sqrt{s} = 0.5, 1.5, 3 \text{ TeV}, \quad \mathcal{L} = 230, 320, 590 \text{ fb}^{-1}$		
C. L.	$ \mu_{\nu_\tau}(\mu_B) $	$ d_{\nu_\tau}(ecm) $
2σ	$(10.90, 5.70, 3.50) \times 10^{-7}$	$(2.10, 1.09) \times 10^{-17}, 6.75 \times 10^{-18}$
3σ	$(11.60, 6.10, 3.70) \times 10^{-7}$	$(2.24, 1.18) \times 10^{-17}, 7.14 \times 10^{-18}$

TABLE V: Bounds on the μ_{ν_τ} magnetic moment and d_{ν_τ} electric dipole moment for the process $e^+e^- \rightarrow e^+\gamma^*\gamma^*e^- \rightarrow e^+\nu_\tau\bar{\nu}_\tau e^-$ for $Q^2 = 64 \text{ GeV}^2$, $\sqrt{s} = 0.5, 1.5, 3 \text{ TeV}$ and $\mathcal{L} = 230, 320, 590 \text{ fb}^{-1}$ at 2σ and 3σ C. L.

$\sqrt{s} = 0.5, 1.5, 3 \text{ TeV}, \quad \mathcal{L} = 230, 320, 590 \text{ fb}^{-1}$		
C. L.	$ \mu_{\nu_\tau}(\mu_B) $	$ d_{\nu_\tau}(ecm) $
2σ	$(9.90, 5.20, 3.10) \times 10^{-7}$	$(1.91, 1.00) \times 10^{-17}, 5.98 \times 10^{-18}$
3σ	$(10.60, 5.54, 3.40) \times 10^{-7}$	$(2.04, 1.07) \times 10^{-17}, 6.56 \times 10^{-18}$

III. CONCLUSIONS

Even though γe^- and $\gamma\gamma$ processes require new equipments, γ^*e^- and $\gamma^*\gamma^*$ are realized spontaneously at linear colliders without any equipments. These processes will allow the next generation linear collider to operate in three different modes, e^+e^- , γ^*e^- and $\gamma^*\gamma^*$, opening up the opportunity for a wider search for new physics. Therefore, the γ^*e^- and $\gamma^*\gamma^*$ linear collisions represents a excellent opportunity to study the sensibility on the anomalous magnetic moment and electric dipole moment of the tau-neutrino.

We have done an analysis of the total cross-section of the processes $e^+e^- \rightarrow e^+\gamma^*e^- \rightarrow e^+\tau\bar{\nu}_\tau\nu_e$ and $e^+e^- \rightarrow e^+\gamma^*\gamma^*e^- \rightarrow e^+\nu_\tau\bar{\nu}_\tau e^-$ as a function of the anomalous coupling F_2 and F_3 . The analysis is shown in Figs. 5, 6, 10 and 11 for different center-of-mass energies and several values of the Weizsacker-Williams photon virtuality. In all case, the cross-section shown a strong dependence on the anomalous couplings F_2 and F_3 .

The correlation between the luminosity \mathcal{L} of the collider and the anomalous magnetic moment μ_{ν_τ} and the electric dipole moment d_{ν_τ} is presented in Figs. 7 and 8. In both case, we see that there is a strong correlation between \mathcal{L} and the dipole moments, the same is also observed in Figs. 12 and 13 as well as in Tables II-V.

We also include contours plots for the dipole moments at the 95% *C.L.* in the $\mu_{\nu_\tau} - d_{\nu_\tau}$ plane for $Q^2 = 2 \text{ GeV}^2$ and $\sqrt{s} = 0.5, 1.5, 3 \text{ TeV}$ in Figures 9 and 14. The contours are obtained of Tables II-V.

It is worth mentioning that our bounds obtained in Tables II-V on the anomalous magnetic moment for the processes $e^+e^- \rightarrow e^+\gamma^*e^- \rightarrow e^+\tau\bar{\nu}_\tau\nu_e$ and $e^+e^- \rightarrow e^+\gamma^*\gamma^*e^- \rightarrow e^+\nu_\tau\bar{\nu}_\tau e^-$ for $Q^2 = 2, 64 \text{ GeV}^2$, $\sqrt{s} = 0.5, 1.5, 3 \text{ TeV}$ and $\mathcal{L} = 230, 320, 590 \text{ fb}^{-1}$ at 2σ and 3σ C. L. compare favorably with the bounds obtained in Table I by DONUT [10], WA66 [11] and L3 Collaboration [12], as well as the reported by K. Akama, *et al.* [23] $\mu_{\nu_\tau} < O(1.1 \times 10^{-6} \mu_B)$ and R. Escobedo *et al.* [7] $\mu_{\nu_\tau} \leq 2.7 \times 10^{-6} \mu_B$ 95% *C.L.* While in the case of the electric dipole moment our results obtained in Table II-V are improved by one order of magnitude than those reported in the literature $|d_{\nu_\tau}| < O(2 \times 10^{-17} \text{ ecm})$ [23] and $|d_{\nu_\tau}| \leq 5.2 \times 10^{-17} \text{ ecm}$, 95% *C.L.* [7].

In conclusion, we have found that the processes $e^+e^- \rightarrow e^+\gamma^*e^- \rightarrow e^+\tau\bar{\nu}_\tau\nu_e$ and $e^+e^- \rightarrow e^+\gamma^*\gamma^*e^- \rightarrow e^+\nu_\tau\bar{\nu}_\tau e^-$ in the γ^*e^- and $\gamma^*\gamma^*$ collision modes at the high energies and luminosities expected at the ILC/CLIC colliders can be used to probe for bounds on the magnetic moment μ_{ν_τ} and electric dipole moment d_{ν_τ} of the tau-neutrino. In particular, we can appreciate that for integrated luminosities of 590 fb^{-1} and center-of-mass energies of 3 TeV , we derive 95% *C.L.* limits on the dipole moments: $\mu_{\nu_\tau} \leq 1.33 \times 10^{-6} \mu_B$ and $d_{\nu_\tau} \leq 2.56 \times 10^{-17} \text{ ecm}$ for the process $e^+e^- \rightarrow e^+\gamma^*e^- \rightarrow e^+\tau\bar{\nu}_\tau\nu_e$ and of $\mu_{\nu_\tau} \leq 3.4 \times 10^{-7} \mu_B$ and $d_{\nu_\tau} \leq 6.56 \times 10^{-18} \text{ ecm}$ for $e^+e^- \rightarrow e^+\gamma^*\gamma^*e^- \rightarrow e^+\nu_\tau\bar{\nu}_\tau e^-$, better than those reported in the literature.

Acknowledgements

A. G. R. acknowledges support from CONACyT, SNI, PROMEP and PIFI (México).

-
- [1] S. L. Glashow, *Nucl. Phys.* **22**, 579 (1961).
 - [2] S. Weinberg, *Phys. Rev. Lett.* **19**, 1264 (1967).
 - [3] A. Salam, in *Elementary Particle Theory*, Ed. N. Svartholm (Almquist and Wiskell, Stockholm, 1968) 367.
 - [4] K. Fujikawa and R. Shrock, *Phys. Rev. Lett.* **45**, 963 (1980).
 - [5] M. Fukugita and T. Yanagida, *Physics of Neutrinos and Applications to Astrophysics*, (Springer, Berlin, 2003).
 - [6] A. Cisneros, *Astrophys. Space Sci.* **10**, 87 (1971).
 - [7] R. Escribano and E. Massó, *Phys. Lett.* **B395**, 369 (1997).
 - [8] P. Vogel and J. Engel, *Phys. Rev.* **D39**, 3378 (1989).
 - [9] C. Arpesella, *et al.*, [Borexino Collaboration], *Phys. Rev. Lett.* **101**, 091302 (2008).
 - [10] R. Schwinhorst, *et al.*, [DONUT Collaboration], *Phys. Lett.* **B513**, 23 (2001).
 - [11] A. M. Cooper-Sarkar, *et al.*, [WA66 Collaboration], *Phys. Lett.* **B280**, 153 (1992).
 - [12] M. Acciarri *et al.*, [L3 Collaboration], *Phys. Lett.* **B412**, 201 (1997).
 - [13] A. Gutiérrez-Rodríguez, *Advances in High Energy Physics* **2014**, 491252 (2014).
 - [14] K. A. Olive, *et al.*, [Particle Data Group], *Chin. Phys.* **C38**, 090001 (2014).
 - [15] A. Gutiérrez-Rodríguez, *Pramana Journal of Physics* **79**, 903 (2012).
 - [16] A. Gutiérrez-Rodríguez, *Eur. Phys. J.* **C71**, 1819 (2011).
 - [17] C. Aydin, M. Bayar and N. Kilic, *Chin. Phys.* **C32**, 608 (2008).
 - [18] A. Gutiérrez-Rodríguez, *et al.*, *Phys. Rev.* **D74**, 053002 (2006).
 - [19] M. A. Pérez, G. Tavares-Velasco and J. J. Toscano, *Int. J. Mod. Phys.* **A19**, 159 (2004).
 - [20] A. Gutiérrez-Rodríguez, *et al.*, *Phys. Rev.* **D69**, 073008 (2004).
 - [21] A. Gutiérrez-Rodríguez, *et al.*, *Acta Physica Slovaca* **53**, 293 (2003).
 - [22] F. Larios, M. A. Pérez, G. Tavares-Velasco, *Phys. Lett.* **B531**, 231 (2002).
 - [23] K. Akama, T. Hattori and K. Katsuura, *Phys. Rev. Lett.* **88**, 201601 (2002).
 - [24] A. Aydemir and R. Sever, *Mod. Phys. Lett.* **A16** 7, 457 (2001).
 - [25] A. Gutiérrez-Rodríguez, *et al.*, *Rev. Mex. de Fís.* **45**, 249 (1999).
 - [26] J. M. Hernández, *et al.*, *Phys. Rev.* **D60**, 013004 (1999).
 - [27] M. Maya, M. A. Pérez, G. Tavares-Velasco, B. Vega, *Phys. Lett.* **B434**, 354 (1998).

- [28] A. Gutiérrez-Rodríguez, *et al.*, *Phys. Rev.* **D58**, 117302 (1998).
- [29] P. Abreu, *et al.*, [DELPHI Collaboration], *Z. Phys.* **C74**, 577 (1997).
- [30] T. M. Gould and I. Z. Rothstein, *Phys. Lett.* **B333**, 545 (1994).
- [31] H. Grotch and R. Robinet, *Z. Phys.* **C39**, 553 (1988).
- [32] T. Abe, *et al.* (Am. LC Group), arXiv:hep-ex/0106057; G. Aarons *et al.*, (ILC Collaboration), arXiv: 0709.1893 [hep-ph]; J. Brau *et al.*, (ILC Collaboration), arXiv: 0712.1950 [physics.acc-ph]; H. Baer, T. Barklow, K. Fujii *et al.*, arXiv:1306.6352 [hep-ph].
- [33] E. Accomando, *et al.* (CLIC Phys. Working Group Collaboration), arXiv: hep-ph/0412251, CERN-2004-005; D. Dannheim, P. Lebrun, L. Linssen *et al.*, arXiv: 1208.1402 [hep-ex]; H. Abramowicz *et al.*, (CLIC Detector and Physics Study Collaboration), arXiv:1307.5288 [hep-ph].
- [34] V. M. Budnev, I. F. Ginzburg, G. V. Meledin and V. G. Serbo, *Phys. Rep.* **15**, 181 (1975).
- [35] G. Baur, *et al.*, *Phys. Rep.* **364**, 359 (2002).
- [36] K. Piotrkowski, *Phys. Rev.* **D63**, 071502 (2001).
- [37] A. Abulencia, *et al.*, [CDF Collaboration], *Phys. Rev. Lett.* **98**, 112001 (2007).
- [38] T. Aaltonen, *et al.*, [CDF Collaboration], *Phys. Rev. Lett.* **102**, 222002 (2009).
- [39] T. Aaltonen, *et al.*, [CDF Collaboration], *Phys. Rev. Lett.* **102**, 242001 (2009).
- [40] S. Chatrchyan, *et al.*, [CMS Collaboration], *JHEP* **1201**, 052 (2012).
- [41] S. Chatrchyan, *et al.*, [CMS Collaboration], *JHEP* **1211**, 080 (2012).
- [42] V. M. Abazov, *et al.*, [D0 Collaboration], *Phys. Rev.* **D88**, 012005 (2013).
- [43] S. Chatrchyan, *et al.*, [CMS Collaboration], *JHEP* **07**, 116 (2013).
- [44] J. Abdallah, *et al.*, [DELPHI Collaboration], *Eur. Phys. J. C35*, (2004) 159.
- [45] I. Sahin, *Phys. Rev.* **D85**, 033002 (2012).
- [46] I. Sahin and M. Koksal, *JHEP* **03**, 100 (2011).
- [47] Pukhov A, *et al.*, CompHEPa package for evaluation of Feynman diagrams and integration over multiparticle phase space, Report No. INP MSU 98-41/542, arXiv:hep-ph/9908288.

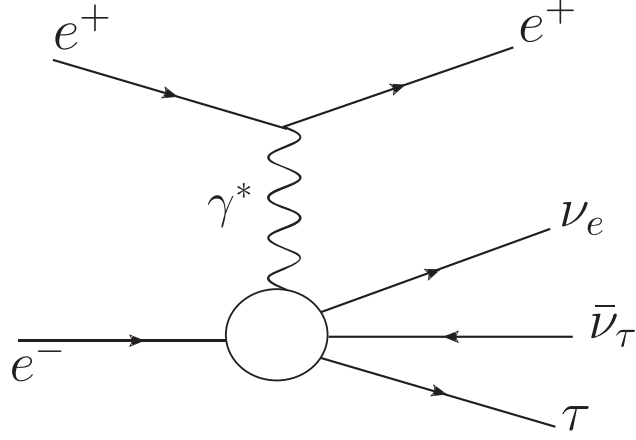


FIG. 1: Schematic diagram for the process $e^+e^- \rightarrow e^+\gamma^*e^- \rightarrow e^+\tau\bar{\nu}_\tau\nu_e$.

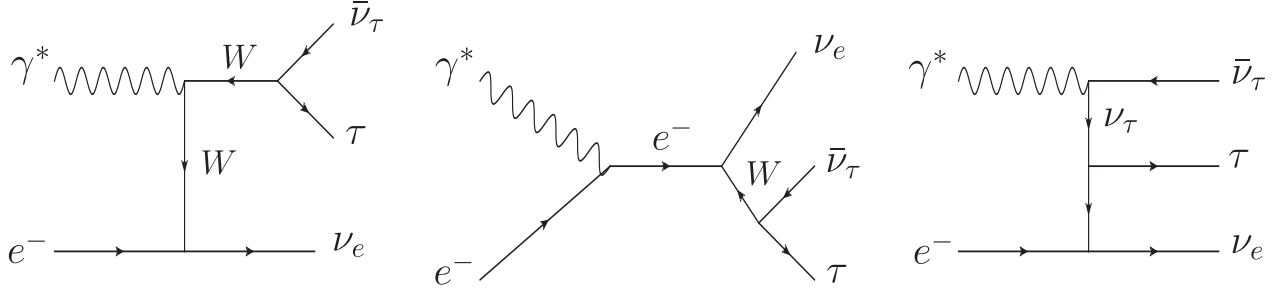


FIG. 2: The Feynman diagrams contributing to the subprocess $\gamma^*e^- \rightarrow \tau\bar{\nu}_\tau\nu_e$.

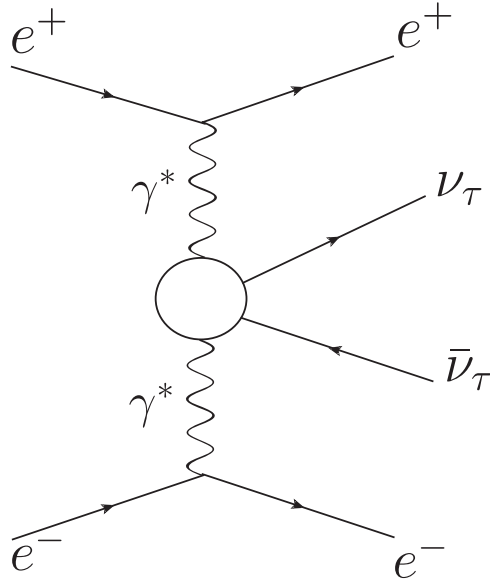


FIG. 3: Schematic diagram for the process $e^+e^- \rightarrow e^+\gamma^*\gamma^*e^- \rightarrow e^+\nu_\tau\bar{\nu}_\tau e^-$.

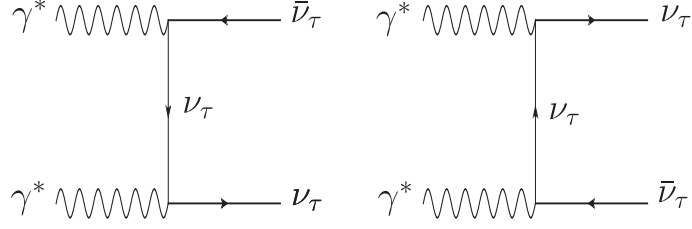


FIG. 4: The Feynman diagrams contributing to the subprocess $\gamma^* \gamma^* \rightarrow \nu_\tau \bar{\nu}_\tau$.

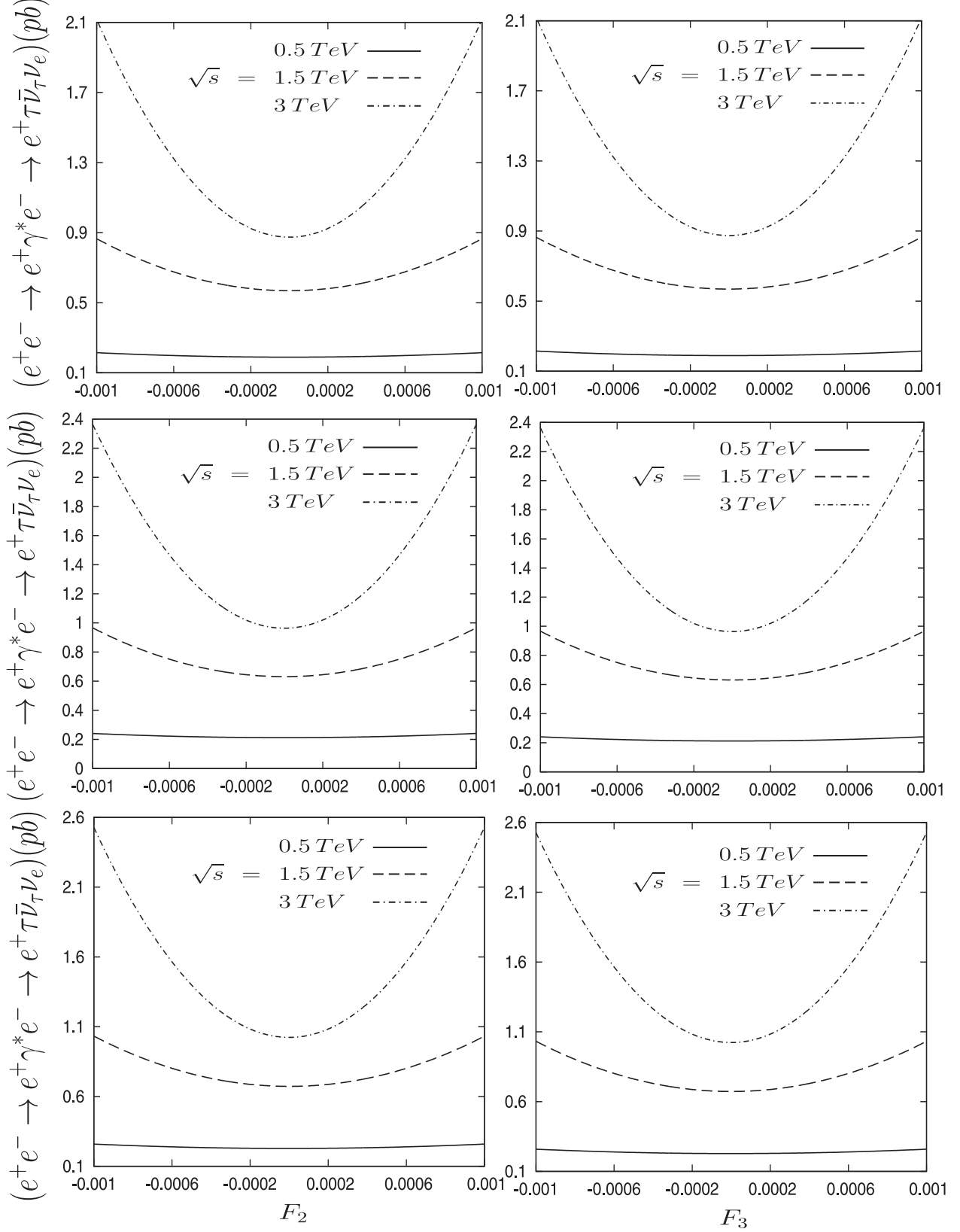


FIG. 5: The integrated total cross-section of the process $e^+e^- \rightarrow e^+\gamma^*e^- \rightarrow e^+\tau\bar{\nu}_\tau\nu_e$ as a function of the anomalous couplings F_2 and F_3 for three different center-of-mass energies $\sqrt{s} = 0.5, 1.5, 3$ TeV and $Q^2 = 2, 16, 64$ GeV², respectively. 14

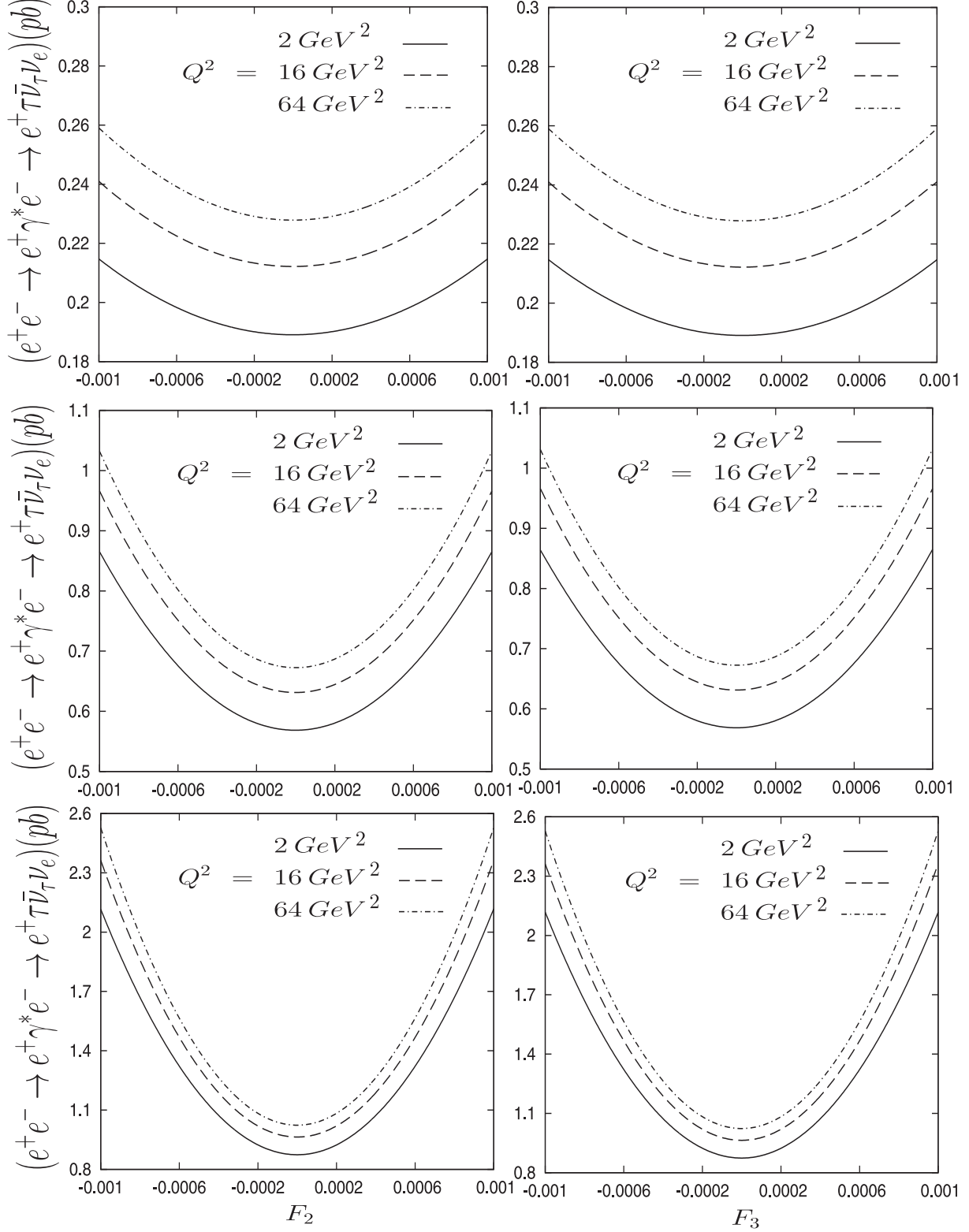


FIG. 6: The total cross section of the process $e^+e^- \rightarrow e^+\gamma^*e^- \rightarrow e^+\tau\bar{\nu}_\tau\nu_e$ as a function of the anomalous couplings F_2 and F_3 for three different values of $Q^2 = 2, 16, 64 \text{ GeV}^2$ and center-of-mass energies $\sqrt{s} = 0.5, 1.5, 3 \text{ TeV}$, respectively.

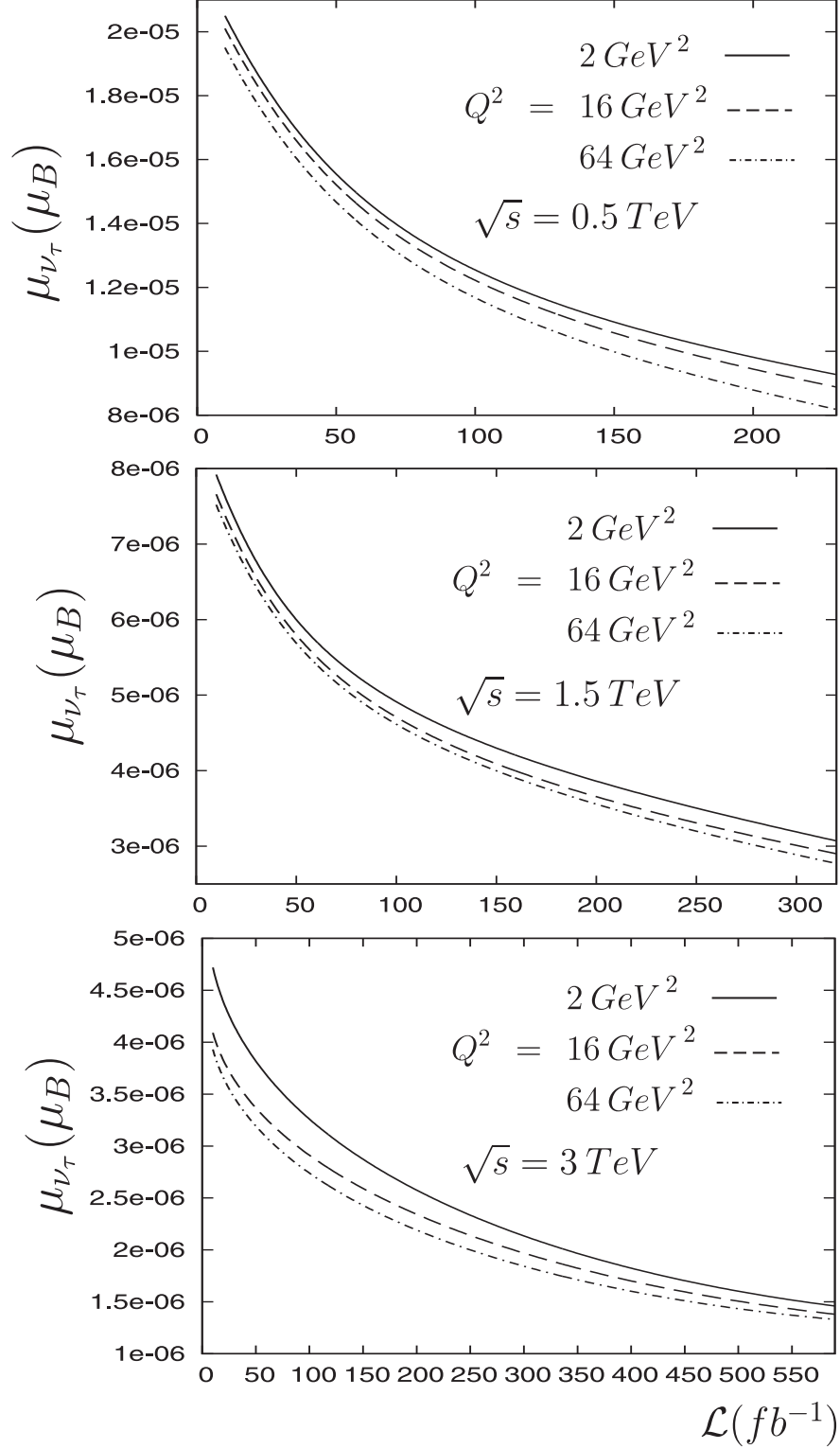


FIG. 7: Dependence of the sensitivity limits at 95% *C.L.* for the anomalous magnetic moment for three different values of $Q^2 = 2, 16, 64 \text{ GeV}^2$ and center-of-mass energies $\sqrt{s} = 0.5, 1.5, 3 \text{ TeV}$ in the subprocess $\gamma^* e^- \rightarrow \tau \bar{\nu}_\tau \nu_e$.

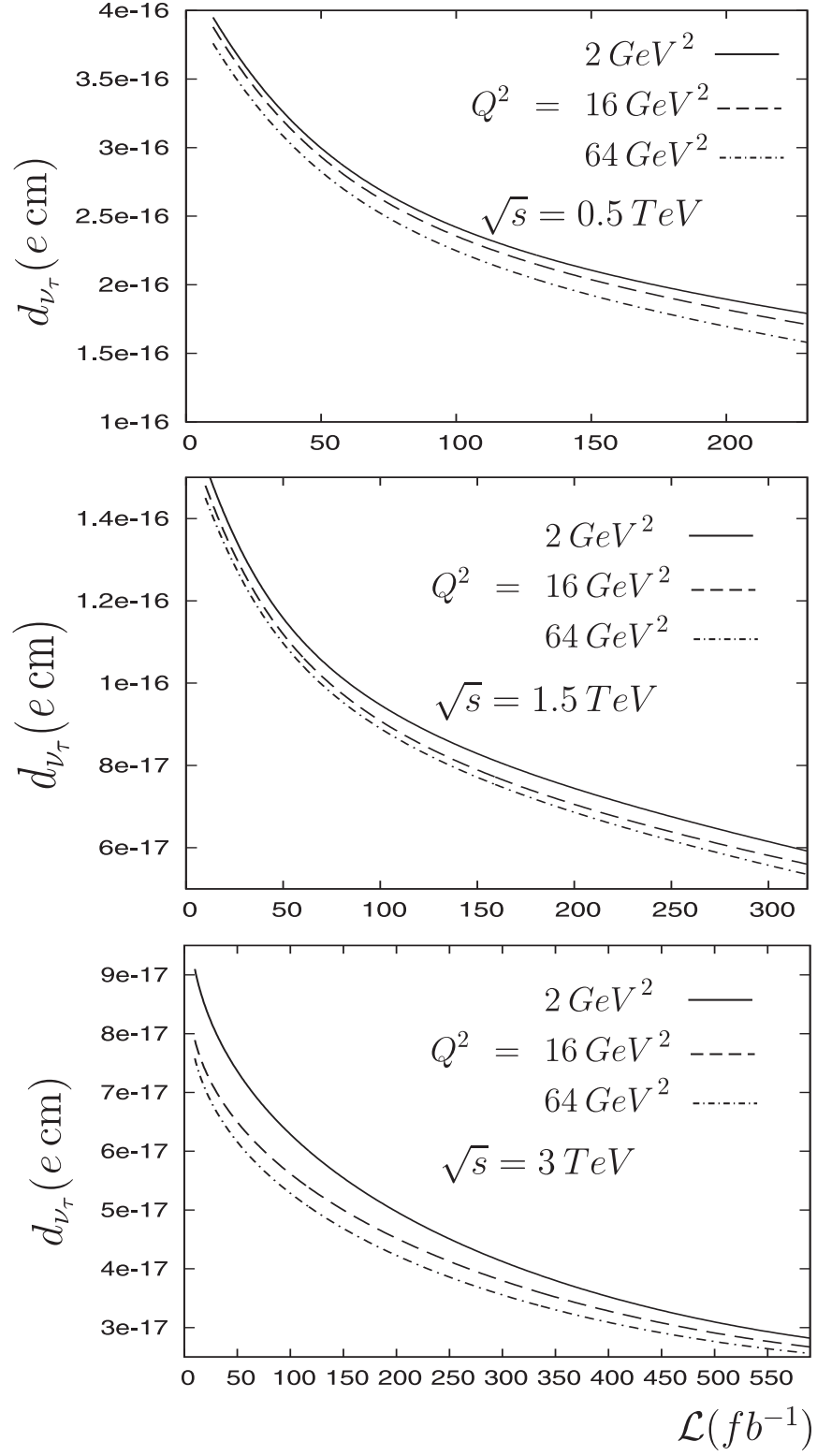


FIG. 8: The same as Fig. 7 but for electric dipole moment.

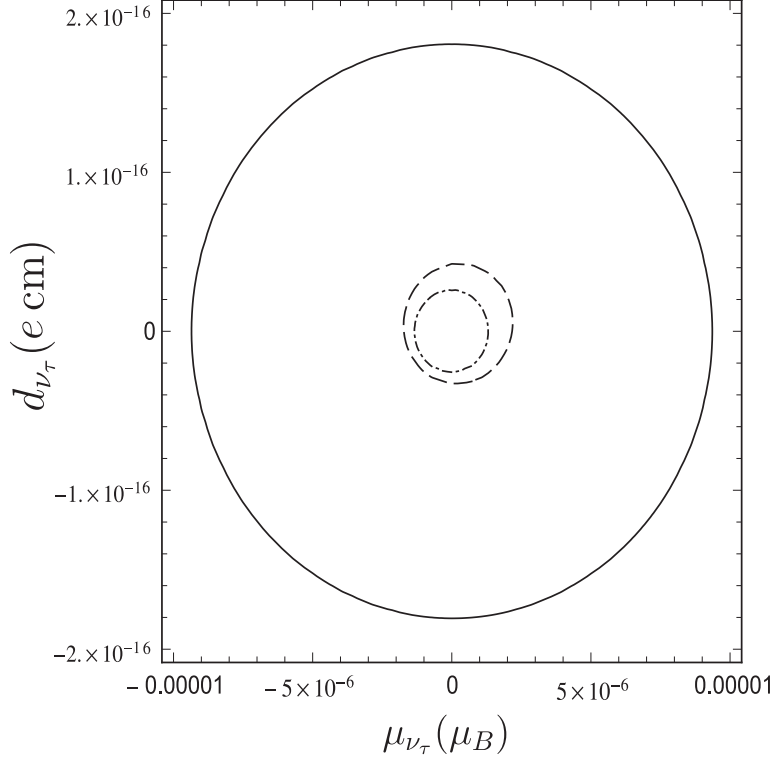


FIG. 9: Limits contours at the 95% *C.L.* in the $\mu_{\nu_\tau} - d_{\nu_\tau}$ plane for $e^+e^- \rightarrow e^+\gamma^*e^- \rightarrow e^+\tau\bar{\nu}_\tau\nu_e$. Starting from the top, the curves are for $\sqrt{s} = 0.5 \text{ TeV}$ and $\mathcal{L} = 230 \text{ fb}^{-1}$; $\sqrt{s} = 1.5 \text{ TeV}$ and $\mathcal{L} = 320 \text{ fb}^{-1}$; $\sqrt{s} = 3 \text{ TeV}$ and $\mathcal{L} = 590 \text{ fb}^{-1}$, respectively. We have used $Q^2 = 2 \text{ GeV}^2$.

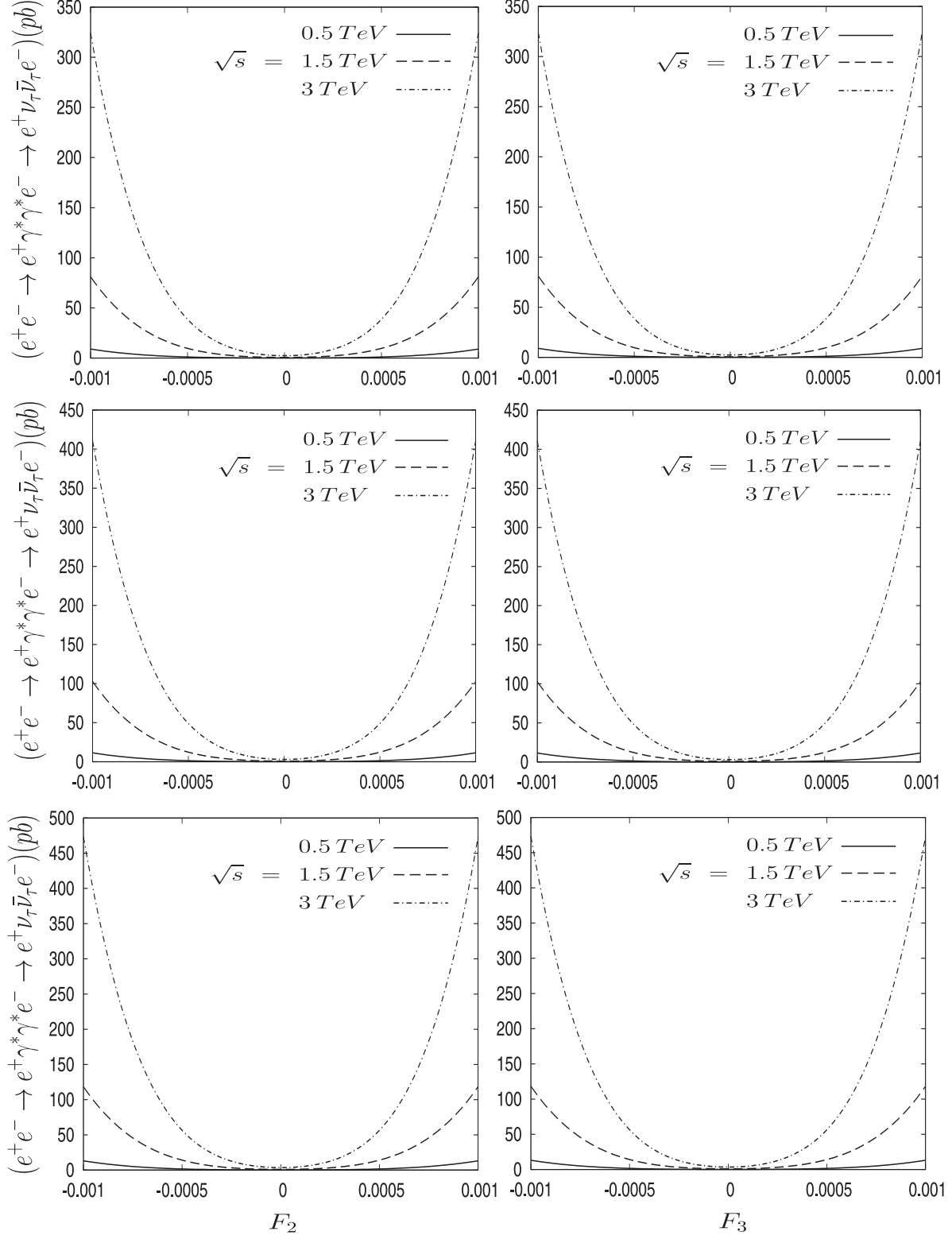


FIG. 10: The total cross section of the process $e^+e^- \rightarrow e^+\gamma^*\gamma^*e^- \rightarrow e^+\nu_\tau\bar{\nu}_\tau e^-$ as a function of the anomalous couplings F_2 and F_3 for three different center-of-mass energies $\sqrt{s} = 0.5, 1.5, 3 \text{ TeV}$ and $Q^2 = 2, 16, 64 \text{ GeV}^2$, respectively.

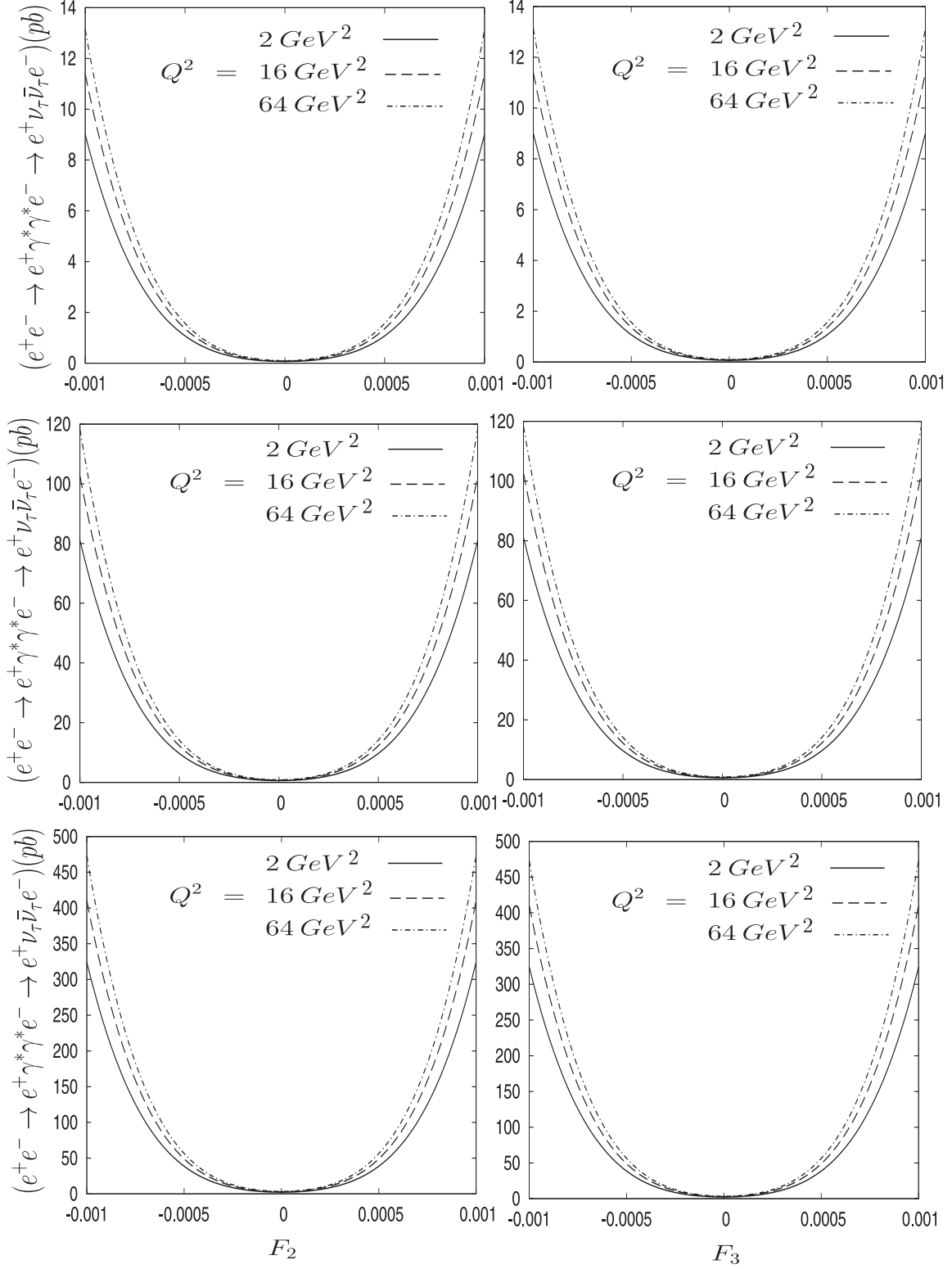


FIG. 11: The integrated total cross-section of the process $e^+e^- \rightarrow e^+\gamma^*\gamma^*e^- \rightarrow e^+\nu_\tau\bar{\nu}_\tau e^-$ as a function of the anomalous couplings F_2 and F_3 for three different values of $Q^2 = 2, 16, 64 \text{ GeV}^2$ and center-of-mass energies $\sqrt{s} = 0.5, 1.5, 3 \text{ TeV}$, respectively.

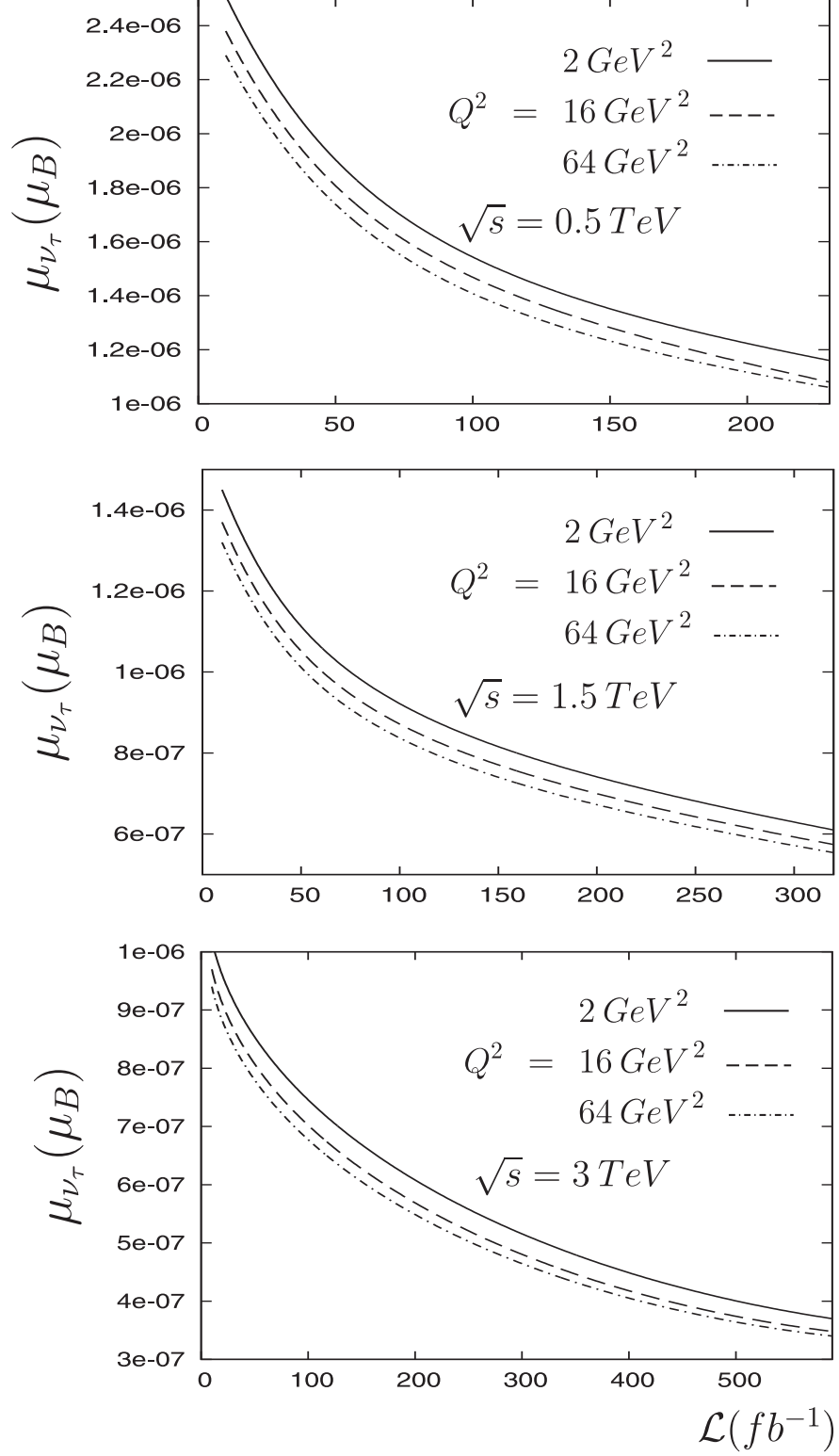


FIG. 12: Dependence of the sensitivity limits at 95% *C.L.* for the anomalous magnetic moment for three different values of $Q^2 = 2, 16, 64 \text{ GeV}^2$ and center-of-mass energies $\sqrt{s} = 0.5, 1.5, 3 \text{ TeV}$ in the subprocess $\gamma^*\gamma^* \rightarrow \nu_\tau\bar{\nu}_\tau$.

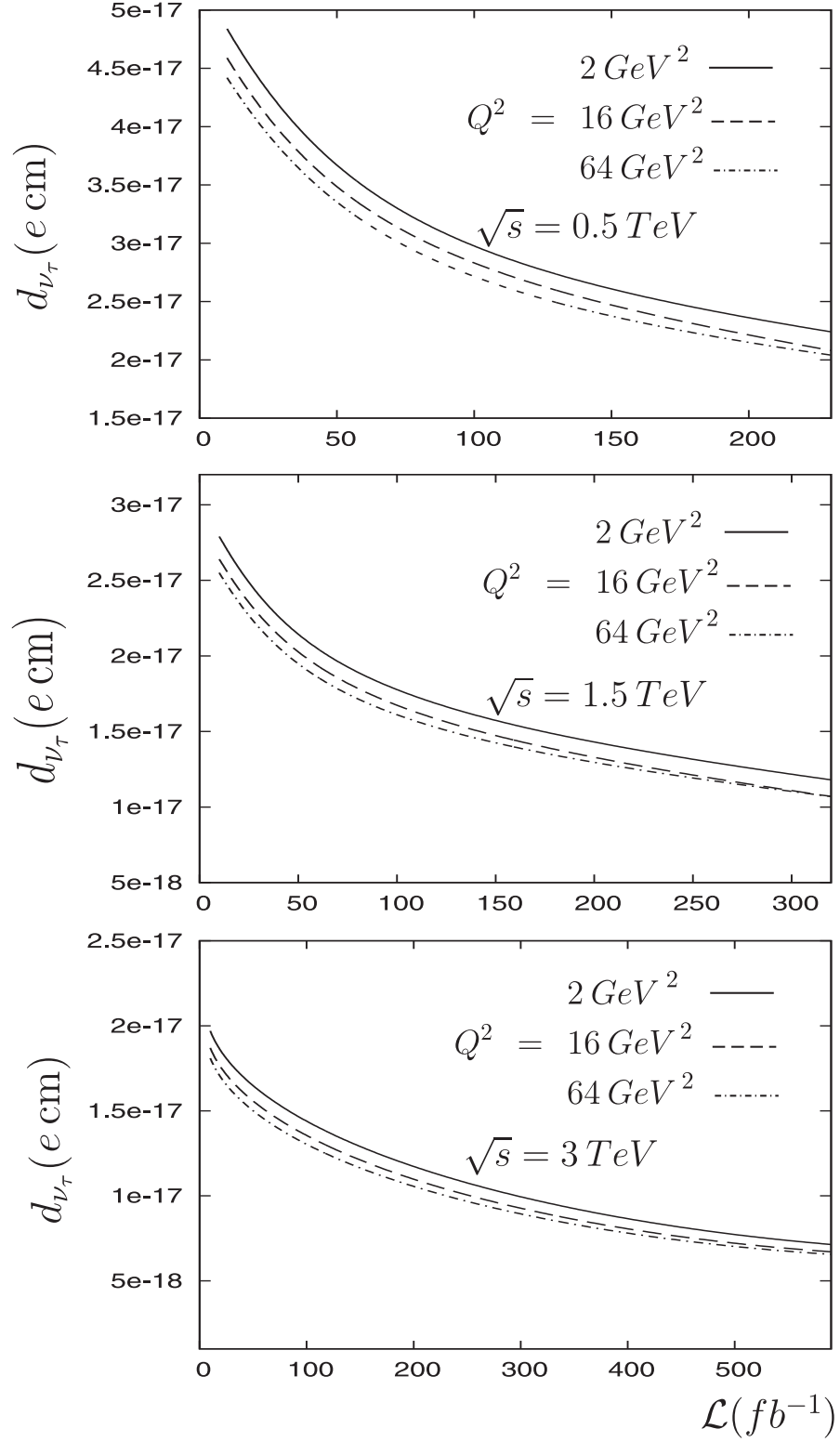


FIG. 13: The same as Fig. 12 but for electric dipole moment.

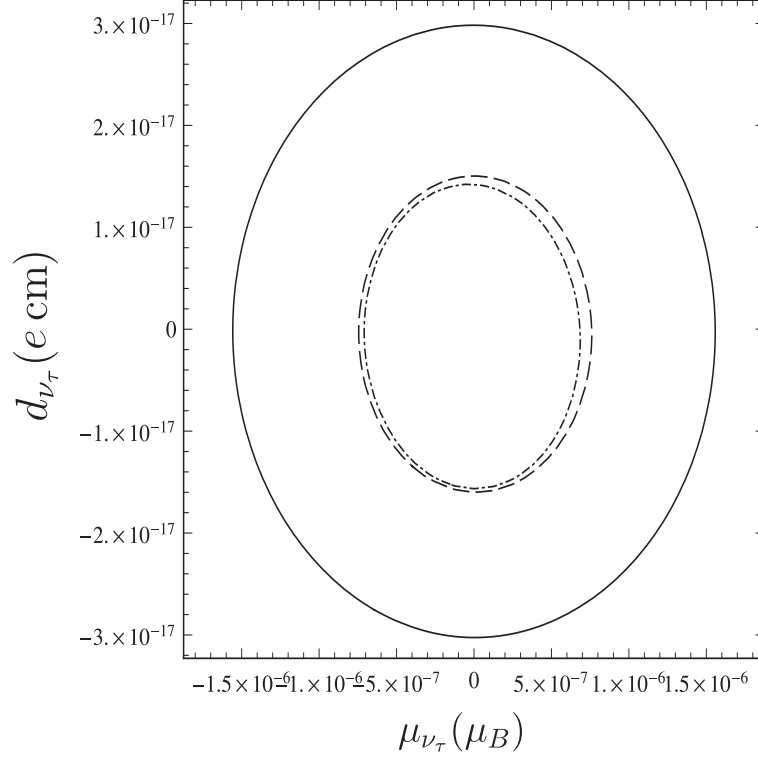


FIG. 14: Limits contours at the 95% *C.L.* in the $\mu_{\nu_\tau} - d_{\nu_\tau}$ plane for $e^+e^- \rightarrow e^+\gamma^*\gamma^*e^- \rightarrow e^+\nu_\tau\bar{\nu}_\tau e^-$. Starting from the top, the curves are for $\sqrt{s} = 0.5 \text{ TeV}$ and $\mathcal{L} = 230 \text{ fb}^{-1}$; $\sqrt{s} = 1.5 \text{ TeV}$ and $\mathcal{L} = 320 \text{ fb}^{-1}$; $\sqrt{s} = 3 \text{ TeV}$ and $\mathcal{L} = 590 \text{ fb}^{-1}$, respectively. We have used $Q^2 = 2 \text{ GeV}^2$.